JACS ARTICLES

Published on Web 06/10/2010

Coaxial Heterogeneous Structure of TiO_2 Nanotube Arrays with CdS as a Superthin Coating Synthesized via Modified Electrochemical Atomic Layer Deposition

Wen Zhu,* Xi Liu, Huiqiong Liu, Dali Tong, Junyou Yang, and Jiangying Peng

State Key Laboratory of Material Processing and Die & Mould Technology, Huazhong University of Science & Technology, Wuhan 430074, People's Republic of China

Received March 25, 2010; E-mail: wennar@mail.hust.edu.cn

Abstract: We report the fabrication and characterization of CdS/TiO_2 nanotube-array coaxial heterogeneous structures. Such structures may potentially be applied in various photocatalytic fields, such as water photocatalytic decomposition and toxic pollutant photocatalytic degradation. Thin films of CdS are conformally deposited onto TiO_2 nanotubes using a modified method of electrochemical atomic layer deposition. We propose that such nanostructured electrodes can overcome the poor absorption and high charge-carrier recombination observed with nanoparticulate films. The practical electrochemical deposition technique promotes the deposition of CdS onto the TiO_2 tube walls while minimizing deposition at the tube entrances, thus preventing pore clogging. The coaxial heterogeneous structure prepared by the new electrochemical process significantly enhances CdS/TiO_2 and CdS/electrolyte contact areas and reduces the distance that holes and electrons must travel to reach the electrolyte or underlying conducting substrate. This results in enhanced photon absorption and photocurrent generation. The detailed synthesis process and the surface morphology, structure, elemental analysis, and photoelectrochemical properties of the resulting films with the CdS/TiO_2 nanotube-array coaxial heterogeneous structure are discussed. In comparison with a pure TiO_2 nanotube array, a 5-fold enhancement in photoactivity was observed using the coaxial heterogeneous structure. This methodology may be useful in designing multijunction semiconductor materials for coating of highly structured substrates.

Introduction

In recent years, the energy crisis and environmental pollution have become two major bottleneck problems that hinder the development of society. Photocatalytic technology is expected to be an effective pathway for solving these problems. The photocatalytic decomposition of water, which uses solar energy to split water, providing clean hydrogen energy, is believed to be able to solve the crisis of fossil fuel depletion, while the photocatalytic degradation of toxic organic pollutants is thought to be an inexpensive and feasible way of addressing environmental issues. In 1972, Fujishima and Honda[1] were the first to report the use of a single-crystal TiO_2 semiconductor photoanode for the photocatalytic decomposition of water. In 1976, Carey et al.[2] successfully used TiO_2 to photocatalytically degrade organic pollutants. TiO_2 photocatalysts thus quickly attracted the attention of global environment and energy researchers. Among all of the TiO_2 nanostructured materials studied in the last three decades, vertically oriented TiO_2 nanotubes (NTs) prepared on a Ti foil by the electrochemical anodization method have become exceedingly in demand.[3−5] These highly ordered NTs offer large specific surface areas without a concomitant decrease in geometric and structural order. Large specific surface areas are well-suited for fully capturing solar energy, and they make available a larger number of active reaction sites for chemical reactions to occur and photogenerated holes to access a large number of solution ions.[6−9] Under UV irradiation, photogenerated electrons can quickly enter the conductive substrate of the TiO_2 NTs, thereby considerably reducing the photogenerated electron and hole recombination possibilities and showing good optical catalytic activity.[10−18] Because TiO_2 is a large-band-gap semiconductor (3.0 and 3.2 eV for the rutile and anatase phases, respectively), its activation is limited only in the UV region, which accounts for only 4−5% of the spectrum of solar energy.[19] Efforts to shift the band gap of TiO_2 while maintaining its excellent charge-transfer properties and photocorrosion stability have primarily focused on metal/nonmetal ion doping to induce a red shift in the band gap.[20,21] Ion doping introduces midgap energy levels; beyond a minimal concentration, however, the doped ions serve as recombination centers

(1) Fujishima, A.; Honda, K. *Nature* **1972**, *238*, 37.
(2) Carey, J. H.; Lawrence, J.; Tosine, H. M. *Bull. Environ. Contam. Toxicol.* **1976**, *16*, 697.
(3) Grimes, C. A.; Mor, G. K. *TiO_2 Nanotube Arrays: Synthesis, Properties, and Applications*; Springer: Berlin, 2009.
(4) Grimes, C. A. *J. Mater. Chem.* **2007**, *17*, 1451.
(5) Mor, G. K.; Prakasam, H. E.; Varghese, O. K.; Shankar, K.; Grimes, C. A. *Nano Lett.* **2007**, *7*, 2356.
(6) Mor, G. K.; Varghese, O. K.; Wilke, R. H. T.; Sharma, S.; Shankar, K.; Latempa, T. J.; Choi, K. S.; Grimes, C. A. *Nano Lett.* **2008**, *8*, 1906.
(7) Kim, D.; Ghicov, A.; Albu, S. P.; Schmuki, P. *J. Am. Chem. Soc.* **2008**, *130*, 16454.
(8) Mohapatra, S. K.; Kondamudi, N.; Banerjee, S.; Misra, M. *Langmuir* **2008**, *24*, 11276.
(9) Feng, X. J.; Shankar, K.; Varghese, O. K.; Paulose, M.; Latempa, T. J.; Grimes, C. A. *Nano Lett.* **2008**, *8*, 3781.

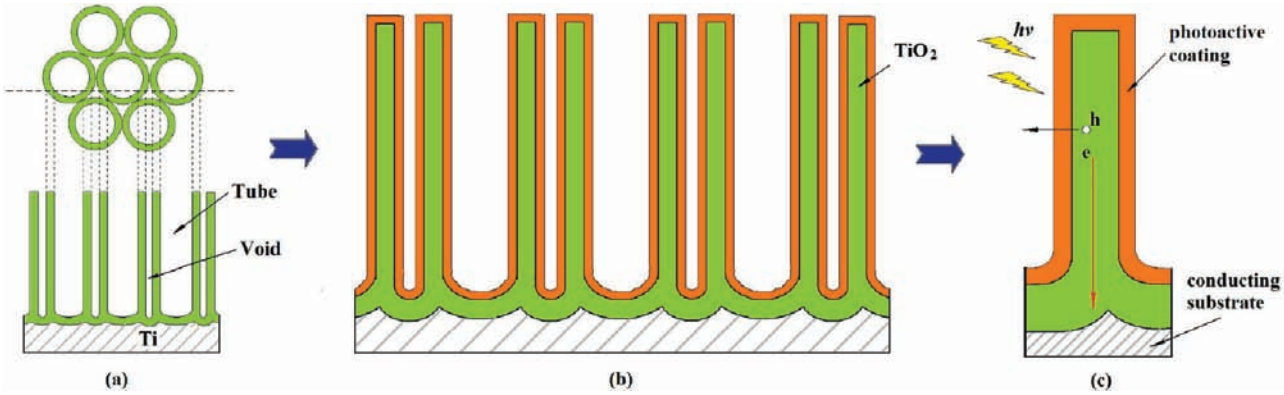

Figure 1. Schematic of narrow-band-gap semiconductor/TiO_2 NT coaxial heterogeneous structural design. (a) Illustration of pure TiO_2 NTs. (b) Cross section of an array of TiO_2 NTs coated with the narrow-band-gap sensitization phase. (c) Cross section of a single coated coaxial heterogeneous structure showing the charge-transfer mechanism. A narrow-band-gap photoactive semiconductor is coated onto the TiO_2 NT substrate to optimize its absorption and charge-transfer properties. Photons ($h\nu$) are absorbed by the sensitization layer, producing electron−hole (e−h) pairs. The holes travel only short distances to reach the electrolyte. The electrons are conducted through the core material to the conducting substrate.

for photogenerated electron−hole pairs.[22] Therefore, extending the photoresponse of TiO_2 NTs to visible light and increasing their photocatalytic efficiency remain possible future research foci.

It was recently reported that the photoactivity of TiO_2 NTs can be enhanced by sensitizing them with a narrow-band-gap semiconductor material such as CdS.[23] In the CdS/TiO_2 NT integrated system, the conduction band of TiO_2 is more anodic than the corresponding band of the sensitizer. The photoelectrons generated in the CdS conduction band move to the conduction band of the TiO_2 NTs and are then transferred to the solution (through back-contact), thereby reducing protons and generating hydrogen. The holes (from both CdS and TiO_2) move to the interface to react with the electrolyte to generate protons. Thus, the thermodynamic conditions necessary for CdS and TiO_2 to match are favorable to electron injections.[24,25] In addition to the band-edge positions of the two semiconductors, the architecture of the composite material also plays a critical role in determining the resultant photoconversion efficiency. The conventional methods for integrating sensitizers to TiO_2 NTs include dipping, the hybrid sol−gel method, hydrothermal synthesis, and electrochemical codeposition.[26−29] In general, these methods easily lead to the precipitation of the sensitizer inside the TiO_2 NTs or even plugging of the nanotubes, resulting in decreases in the specific surface area and adsorption capacity.[30,31] Ideally, a suitable architecture for the integrated material is one that meets the requirements for the following parameters: (1) the surface structure, (2) the geometrical structure, and (3) the contact form.

With regard to the surface structure, in principle, the narrow-band-gap sensitization phase must evenly cover the TiO_2 NT walls, forming a coaxial heterogeneous structure (Figure 1). Figure 1a shows an illustration of the pure TiO_2 NTs. A cross section of an array of coated TiO_2 NTs with the narrow band gap sensitization phase is shown in Figure 1b, while a cross section of a single coated coaxial heterogeneous structure showing the charge-transfer mechanism is displayed in Figure 1c. The incident light ($h\nu$) is absorbed by the sensitization layer and produces an electron−hole (e−h) pair. The holes migrate to the sensitizer−electrolyte interface and participate in the oxygen production reaction of water splitting. The electrons are transferred to the core material and travel to the back-contact, where they are conducted around the circuit to the counter electrode to participate in the hydrogen production reaction. Such a structure is designed to help improve the contact area between the sensitizer and the TiO_2 surface, exciting the photoelectrons in the sensitizer and smoothly injecting them into the conduction band of TiO_2 NTs. This surface structure also does not reduce the specific surface area and adsorption capacity of the TiO_2 NTs.

With regard to the geometrical structure, the recombination of the photogenerated e−h pairs can be minimized by precisely controlling the relevant geometric thickness of the sensitization

(10) Shankar, K.; Bandara, J.; Paulose, M.; Wietasch, H.; Varghese, O. K.; Mor, G. K.; Latempa, T. J.; Thelakkat, M.; Grimes, C. A. *Nano Lett.* **2008**, *8*, 1654.
(11) Allam, N. K.; Shankar, K.; Grimes, C. A. *Adv. Mater.* **2008**, *20*, 3942.
(12) Allam, N. K.; Grimes, C. A. *Langmuir* **2009**, *25*, 7234.
(13) Liu, Z. Y.; Subramania, V. R.; Misra, M. *J. Phys. Chem. C* **2009**, *113*, 14028.
(14) Macak, J. M.; Albu, S.; Kim, D. H.; Paramasivam, I.; Aldabergerova, S.; Schmuki, P. *Electrochem. Solid-State Lett.* **2007**, *10*, K28.
(15) Albu, S. P.; Ghicov, A.; Aldabergenova, A.; Drechsel, P.; LeClere, D.; Thompson, G. E.; Macak, J. M.; Schmuki, P. *Adv. Mater.* **2008**, *20*, 4135.
(16) John, S. E.; Mohapatra, S. K.; Misra, M. *Langmuir* **2009**, *25*, 8240.
(17) Mohapatra, S. K.; Raja, K. S.; Mahajan, V. K.; Misra, M. *J. Phys. Chem. C* **2008**, *112*, 11007.
(18) Shankar, K.; Basham, J. I.; Allam, N. K.; Varghese, O. K.; Mor, G. K.; Feng, X. J.; Paulose, M.; Seabold, J. A.; Choi, K. S.; Grimes, C. A. *J. Phys. Chem. C* **2009**, *113*, 6327.
(19) Mor, G. K.; Varghese, O. K.; Paulose, M.; Shankar, K.; Grimes, C. A. *Sol. Energy Mater. Sol. Cells* **2006**, *90*, 2011.
(20) Khan, M. A.; Yang, O. B. *Catal. Today* **2009**, *146*, 177.
(21) Liu, Z. Y.; Pesic, B.; Raja, K. S.; Rangaraju, R. R.; Misra, M. *Int. J. Hydrogen Energy* **2009**, *34*, 3250.
(22) Maeda, K.; Domen, K. *J. Phys. Chem. C* **2007**, *111*, 7851.
(23) Chen, S.; Paulose, M.; Ruan, C.; Mor, G. K.; Varghese, O. K.; Kouzoudis, D.; Grimes, C. A. *J. Photochem. Photobiol., A* **2006**, *177*, 177.
(24) Bai, J.; Li, J. H.; Liu, Y. B.; Zhou, B. X.; Cai, W. M. *Appl. Catal., B* **2010**, *95*, 408.
(25) Zhang, J. L.; Zhang, X. W.; Lei, L. C. *Chin. Sci. Bull.* **2008**, *53*, 1929.
(26) Zhang, H.; Quan, X.; Chen, S.; Yu, H. T.; Ma, N. *Chem. Mater.* **2009**, *21*, 3090.
(27) Banerjee, S.; Mohapatra, S. K.; Das, P. P.; Misra, M. *Chem. Mater.* **2008**, *20*, 6784.
(28) Sun, W. T.; Yu, Y.; Pan, H. Y.; Gao, X. F.; Chen, Q.; Peng, L. M. *J. Am. Chem. Soc.* **2008**, *130*, 1124.
(29) Shin, K.; Seok, S. i.; Im, S. H.; Park, J. H. *Chem. Commun.* **2010**, *46*, 2385.
(30) Yin, Y. X.; Jin, Z. G.; Hou, F. *Nanotechnology* **2007**, *18*, 495608.
(31) Seabold, J. A.; Shankar, K.; Wilke, R. H. T.; Paulose, M.; Varghese, O. K.; Grimes, C. A.; Choi, K. S. *Chem. Mater.* **2008**, *20*, 5266.

layer, thereby reducing the distance that holes and electrons must travel in the sensitization layer to reach the electrolyte or underlying conducting substrate. In particular, when the geometric thickness of the sensitization layer is smaller than the width of the space-charge layer, the photogenerated hole and electron are unable to recombine and separately reach the electrolyte solution and the underlying conducting substrate, respectively. This enables minimal charge-carrier recombination.

With regard to the contact form, good interactions between the sensitization phase and the TiO_2 NTs lead to efficient and rapid charge transfer through the coupled semiconductor. In particular, when the contact form between the sensitization phase and TiO_2 NTs has better Ohmic contact, the charge is transferred more smoothly and separation proceeds more easily, resulting in higher photocatalytic efficiency.

These three requirements are difficult to achieve using the conventional method for preparing heterojunctions. A novel electrochemical method, called electrochemical atomic layer deposition, can meet these conditions.

Electrochemical atomic layer deposition (ALD), previously known as electrochemical atomic layer epitaxy (EC-ALE), was put forward by Stickney and co-workers.[32−34] Electrochemical ALD has been used to grow structurally well-ordered compound semiconductors with atomic-level control under ambient temperature and pressure.[35−53] It is based on the alternating underpotential deposition (UPD) of the elements that form the compound semiconductor in a cycle. UPD is a surface-limited phenomenon, so the resulting deposit is generally limited to an atomic layer.[54−56] Thus, as long as the deposition potential is controlled in the UPD range, the deposition atoms can only be grown on the top of the heterogeneous atoms. After the underlying heterogeneous atoms are completely covered by the deposited atoms, continued growth would have to occur on top of the homogeneous atoms. However, because the deposition potential is controlled in the UPD range, the driving force is not sufficient to grow atoms on top of the homogeneous atoms; thus, the growth process stops, thereby avoiding bulk-phase or island deposition. Therefore, each deposition cycle can form only a monolayer of heterogeneous elements, and the thickness of the deposit is controlled by the number of deposition cycles.[57,58] This growth mechanism ensures morphological consistency between the deposition layer surface and the underlying substrate surface.

Using electrochemical ALD to prepare the coaxial heterogeneous structure based on TiO_2 NTs features significant advantages in the surface and geometrical structures, contact form, and so on. First, because of the atomic monolayer growth mechanism of electrochemical ALD, the heterogeneous deposition layer can evenly cover the set area or complex shapes. In other words, the deposition layer conforms to the underlying substrate and does not encounter the phenomenon of plugging of the nanotubes. Second, by restricting the number of cycles and the deposition time, the thickness of the deposition films can be precisely controlled. As a result, coaxial heterogeneous structures within a superthin coating can be obtained, which is favorable for reducing the charge-carrier recombination probability. Third, electrochemical ALD gives rise to good interactions between the deposition layer and the NTs (the interface properties from the atom-by-atom contact form) and as a result enables efficient and rapid charge transfer through the coupled semiconductor. Yet another advantage of using electrochemical ALD to prepare the coaxial heterogeneous structure based on TiO_2 NTs is that metallic or nonmetallic doping can be more conveniently achieved simply by changing the deposition solution. With the special technology involved in electrochemical ALD, the doping element can directly enter the crystal lattice of the deposition layer through the atomic layer. The grain boundaries (as recombination centers) can be minimized, thereby effectively improving the photocatalytic performance.

In the electrochemical ALD method, separate solutions and potentials are used to electrochemically deposit atomic layers of each element in a cycle.[59] The electrode is rinsed using a blank solution after each UPD deposition, which can be performed through an automated solution conversion system. In general, an electrode with a flat, smooth surface is often used in this method.[60,61] A flat surface is also favorable for the rinsing process. The electrode used in this work was composed of TiO_2

(32) Gregory, B. W.; Stickney, J. L. *J. Electroanal. Chem.* **1991**, *300*, 543.
(33) Stickney, J. L. *J. Electroanal. Chem.* **1999**, *21*, 75.
(34) Thambidurai, C.; Kim, Y. G.; Stickney, J. L. *Electrochim. Acta* **2008**, *53*, 6157.
(35) Stickney, J. L. *Advances in Electrochemical Science and Engineering*; Kolb, D. M., Alkire, R., Eds.; Wiley-VCH: Weinheim, Germany, 2002.
(36) Oznuluer, T.; Demir, U. *J. Electroanal. Chem.* **2002**, *529*, 34.
(37) Demir, U.; Shannon, C. *Langmuir* **1994**, *10*, 2794.
(38) Demir, U.; Shannon, C. *Langmuir* **1996**, *12*, 6091.
(39) Banga, D. O.; Vaidyanathan, R.; Liang, X. H.; Stickney, J. L.; Cox, S.; Happeck, U. *Electrochim. Acta* **2008**, *53*, 6988.
(40) Kim, J. Y.; Stickney, J. L. *J. Phys. Chem. C* **2008**, *112*, 5966.
(41) Thambidurai, C.; Kim, Y. G.; Jayaraju, N.; Venkatasamy, V.; Stickney, J. L. *J. Electrochem. Soc.* **2009**, *156*, D261.
(42) Venkatasamy, V.; Shao, I.; Huang, Q.; Stickney, J. L. *J. Electrochem. Soc.* **2008**, *155*, D693.
(43) Kim, J. Y.; Kim, Y. G.; Stickney, J. L. *J. Electroanal. Chem.* **2008**, *621*, 205.
(44) Kim, Y. G.; Kim, J. Y.; Thambidurai, C.; Stickney, J. L. *Langmuir* **2007**, *23*, 2539.
(45) Kim, Y. G.; Kim, J. Y.; Stickney, J. L. *J. Electrochem. Soc.* **2007**, *154*, D260.
(46) Loglio, F.; Telford, A. M.; Salvietti, E.; Innocenti, M.; Pezzatini, G.; Cammelli, S.; D'Acapito, F.; Felici, R.; Pozzi, A.; Foresti, M. L. *Electrochim. Acta* **2008**, *53*, 6978.
(47) Foresti, M. L.; Loglio, F.; Innocenti, M.; Bellassai, S.; Carla, F.; Lastraioli, E.; Pezzatini, G.; Bianchini, C.; Vizza, F. *Langmuir* **2010**, *26*, 1802.
(48) Cavallini, M.; Facchimi, M.; Albonetti, C.; Biscarini, F.; Innocenti, M.; Loglio, F.; Salvietti, E.; Pezzatini, G.; Foresti, M. L. *J. Phys. Chem. C* **2007**, *111*, 1061.
(49) Salvietti, E.; Loglio, F.; Innocenti, M.; Cavallini, M.; Facchini, M.; Pezzatini, G.; Raiteri, R.; Foresti, M. L. *Electrochim. Acta* **2007**, *52*, 6034.
(50) Zhu, W.; Yang, J. Y.; Zhou, D. X.; Xiao, C. J.; Duan, X. K. *J. Electroanal. Chem.* **2008**, *614*, 41.
(51) Yang, J. Y.; Zhu, W.; Gao, X. H.; Bao, S. Q.; Fan, X. A.; Duan, X. K.; Hou, J. *J. Phys. Chem. B* **2006**, *110*, 4599.
(52) Zhu, W.; Yang, J. Y.; Zhou, D. X.; Xiao, C. J.; Duan, X. K. *Electrochim. Acta* **2008**, *53*, 3579.
(53) Zhu, W.; Yang, J. Y.; Zhou, D. X.; Xiao, C. J.; Duan, X. K. *Langmuir* **2008**, *24*, 5919.
(54) Kolb, D. W. *Advances in Electrochemistry and Electrochemical Engineering*; Gerischer, H., Tobias, C. W., Eds.; Wiley: New York, 1978; p. 125.
(55) Liang, X. H.; Kim, Y. G.; Gebergziabiher, D. K.; Stickney, J. L. *Langmuir* **2010**, *26*, 2877.
(56) Alanyalioglu, M.; Cakal, H.; Ozturk, A. E.; Demir, U. *J. Phys. Chem. B* **2001**, *105*, 10588.
(57) Fernandes, V. C.; Salvietti, E.; Loglio, F.; Lastraioli, E.; Innocenti, M.; Mascaro, L. H.; Foresti, M. L. *J. Appl. Electrochem.* **2009**, *39*, 2191.
(58) Loglio, F.; Innocenti, M.; Jarek, A.; Caporali, S.; Pasquini, I.; Foresti, M. L. *J. Electroanal. Chem.* **2010**, *638*, 15.
(59) Stickney, J. L.; Wade, T. L.; Flowers, B. H., Jr.; Vaidyanathan, R.; Happek, U. *Encyclopedia of Electrochemistry*; Gileadi, E., Urbakh, M., Eds.; Marcel Dekker: New York, 2002.
(60) Zhu, W.; Yang, J. Y.; Zhou, D. X.; Bao, S. Q.; Fan, X. A.; Duan, X. K. *Electrochim. Acta* **2007**, *52*, 3660.

NTs with special surface structures, which made rinsing away the preceding reaction solution with the blank solution difficult because of the large specific surface area of the TiO_2 NTs. The UPD potentials of different elements may not be similar. In some cases, the UPD potential of one element may correspond to the bulk deposition potential of another element. If the preceding reaction solution is not adequately rinsed away, leaving some remnants of the preceding reaction solution when the following reaction solution is introduced, the potential used to deposit the following element in the UPD range may result in bulk-phase or island deposition of the residual preceding element. To overcome this problem, a number of methods for adjusting the UPD potentials of the two species to fall within the same range have been employed. For example, Demir and co-workers[62] recently developed a modified electrochemical ALD method based on codeposition from a solution containing both Pb^{2+} and S^{2-} as well as the disodium salt of ethylenediaminetetraacetic acid (EDTA), a complexing agent, at a constant potential determined from the UPD potentials of Pb and S. This electrochemical method combines UPD and codeposition. To date, this method has been extensively applied to grow highly crystalline thin films of PbS,[62,63] ZnS,[64] CdS,[65] PbTe,[66] and Sb_2Te_3[67] on single-crystalline Au(111). In the present study, we illustrate the growth of CdS nanofilms on TiO_2 NT electrodes to form a coaxial heterogeneous structure through a one-step process using the new electrochemical codeposition method. To determine their morphology, composition, and structure, the deposited films were examined by field-emission scanning electron microscopy (FE-SEM), X-ray diffraction (XRD), and energy-dispersive X-ray spectrophotometry (EDX). This study also provides information on the photoelectrochemical properties of the resulting films having the CdS/TiO_2 nanotube-array coaxial heterogeneous structure.

Results and Discussion

Curve (a) in Figure 2 is the cyclic voltammogram of Cd on TiO_2 NT substrates in the UPD range in an EDTA-free solution at pH 8.5, while curve (b) is the cyclic voltammogram of Cd on TiO_2 NT substrates in solutions containing 10 mM $CdSO_4$ and 0.15 M EDTA at the same pH. In comparison with curve (a), in the presence of EDTA, both the deposition and stripping peak potentials of curve (b) are shifted toward more negative potentials. Curve (c) in Figure 2 shows the cyclic voltammogram of S on TiO_2 NT substrates in 2 mM Na_2S and 0.15 M EDTA at pH 8.5. Figure 2 shows that the UPD potentials of Cd and S on the TiO_2 NTs are transferred to the same region by the addition of EDTA to the precursor solution. If the potential of the electrode is kept constant at an appropriate potential that is in the middle of the common UPD region, then theoretically Cd and S can simultaneously be deposited onto the substrate using UPD. Aside from determining the shift in the UPD potential of metallic cations, the most important role of EDTA here lies in keeping Cd complexed, thereby avoiding the formation of CdS particles in the solution phase that could contribute to film growth. This was also observed by Demir and co-workers when they applied the UPD-based electrochemical technique to obtain thin films of PbS, CdS, ZnS, and PbTe compound semiconductors on Au(111).[62,64−66] Demir's group recently demonstrated a new electrochemical process for obtaining highly oriented PbS thin films without using EDTA. This technique is again based on the UPD of Pb and S from a saturated solution of PbS containing excess PbS particles as a source of Pb^{2+} and S^{2-} at different temperatures.[63] To prepare high-quality CdS/TiO_2 coaxial heterogeneous structures, the deposition potential must be correctly selected to ensure the simultaneous UPD of both Cd and S on the TiO_2 NT electrodes. In this study, we investigated the effects of the deposition potential on the microstructure and characterization of the prepared CdS/TiO_2 coaxial heterogeneous structures. Three different potentials within the common UPD region were selected to determine the optimum deposition potential parameter.

Figures 3−5 show the XRD pattern, EDX spectrum, and FE-SEM micrographs, respectively, of as-prepared CdS/TiO_2 coaxial heterogeneous structures formed using a deposition potential of −0.65 V for 5 h. Only the diffractive peaks of

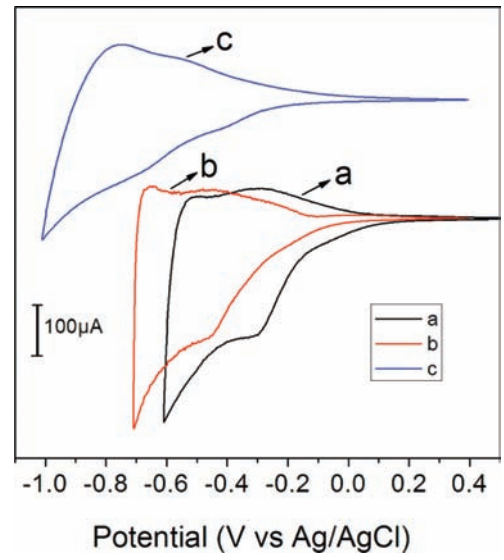

Figure 2. Cyclic voltammograms of TiO_2 nanotube electrodes recorded at 5 mV/s in solutions containing (a) 10 mM $CdSO_4$ and 50 mM Na_2SO_4; (b) 10 mM $CdSO_4$ and 0.15 M EDTA; and (c) 2 mM Na_2S and 0.15 M EDTA.

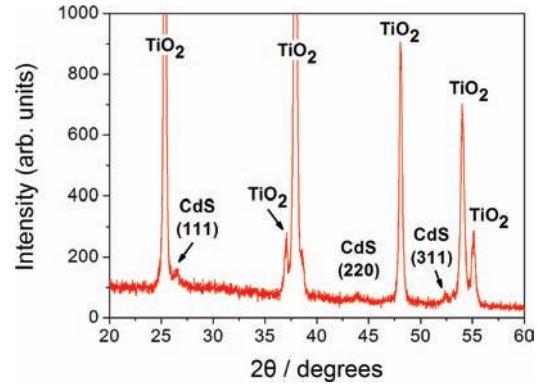

Figure 3. XRD diffractograms of CdS electrodeposited onto TiO_2 NTs at a deposition potential of −0.65 V (vs Ag/AgCl).

(61) Vaidyanathan, R.; Cox, S. M.; Happek, U.; Banga, D.; Mathe, M. K.; Stickney, J. L. *Langmiur* **2006**, *22*, 10590.
(62) Oznuluer, T.; Erdogan, I.; Sisman, I.; Demir, U. *Chem. Mater.* **2005**, *17*, 935.
(63) Alanyalioglu, M.; Bayrakceken, F.; Demir, U. *Electrochim. Acta* **2009**, *54*, 6554.
(64) Oznuluer, T.; Erdogan, I.; Demir, U. *Langmuir* **2006**, *22*, 4415.
(65) Sisman, I.; Alanyalioglu, M.; Demir, U. *J. Phys. Chem. C* **2007**, *111*, 2670.
(66) Erdogan, I. Y.; Oznuluer, T.; Bulbul, F.; Demir, U. *Thin Solid Films* **2009**, *517*, 5419.
(67) Erdogan, I. Y.; Demir, U. *J. Electroanal. Chem.* **2009**, *633*, 253.

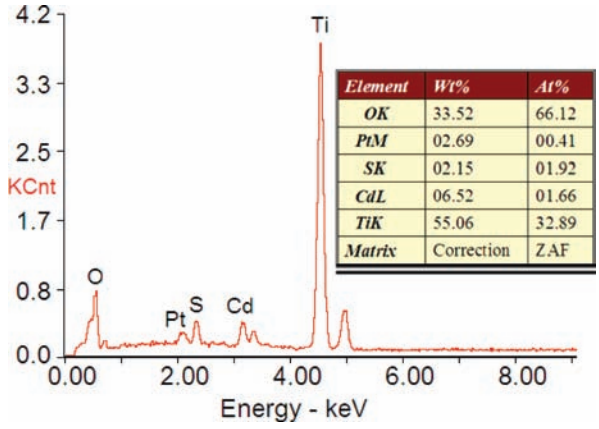

Element	Wt%	At%
OK	33.52	66.12
PtM	02.69	00.41
SK	02.15	01.92
CdL	06.52	01.66
TiK	55.06	32.89
Matrix	Correction	ZAF

Figure 4. EDX spectrum of stoichiometric CdS electrodeposited onto TiO_2 NTs at a deposition potential of −0.65 V (vs Ag/AgCl).

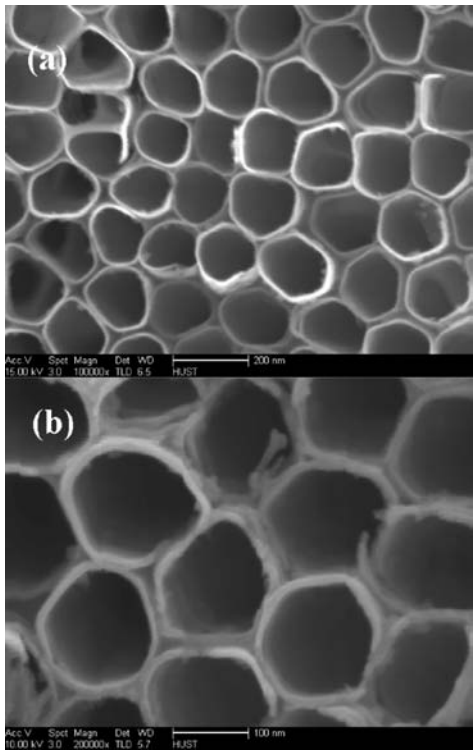

Figure 5. (a) Top-surface FE-SEM micrographs of CdS electrodeposited onto TiO_2 NT arrays at −0.65 V (vs Ag/AgCl). (b) Enlarged micrograph showing a very thin deposition layer grown on the tube wall surface.

single-phase CdS and the TiO_2 substrate without the superfluous peaks of elemental Cd or S were observed (Figure 3). However, as shown in Figure 3, the characteristic peaks of CdS were weak, indicating that the coverage of the electrodeposited coating obtained at −0.65 V was low. EDX quantitative analysis of the coating also gave an approximately 1:1 stoichiometric ratio of Cd to S (Cd, 1.66%; S, 1.92%), as expected for the format of CdS compound (Figure 4). The source of the Pt peak shown in the EDX spectrum was the Pt sprayed onto the sample surface during the FE-SEM experiment to increase its conductivity. Shown in Figure 5a is a low-magnification FE-SEM image of the CdS-deposited nanotube film, which reveals that well-ordered pore structures were maintained. This suggests that the CdS deposition process does not damage the ordered TiO_2 nanotube array structure. The surface morphology of the as-prepared coaxial heterogeneous structures at −0.65 V was

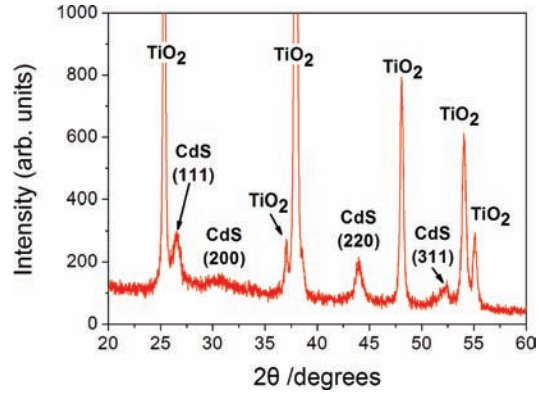

Figure 6. XRD diffractograms of CdS electrodeposited onto TiO_2 NTs at a deposition potential of −0.7 V (vs Ag/AgCl).

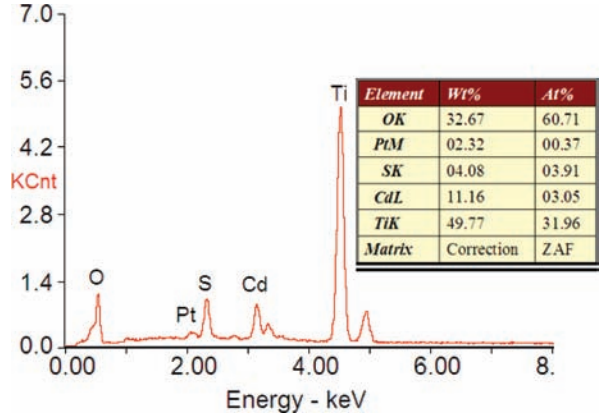

Element	Wt%	At%
OK	32.67	60.71
PtM	02.32	00.37
SK	04.08	03.91
CdL	11.16	03.05
TiK	49.77	31.96
Matrix	Correction	ZAF

Figure 7. EDX spectrum of stoichiometric CdS electrodeposited onto TiO_2 NTs at a deposition potential of −0.7 V (vs Ag/AgCl).

analogous to that of the pure TiO_2 NT substrate. The tube inner diameter and wall thickness and the length of the resulting heterogeneous structure were not significantly different from those of the pure substrate (information regarding the TiO_2 NT morphology parameters is given in the Supporting Information). Closer observations (Figure 5b) reveal that the deposition layer grew on the surface of the tube wall.

The XRD pattern, EDX spectrum, and FE-SEM micrographs of the as-prepared CdS/TiO_2 coaxial heterogeneous structure formed at a deposition potential of −0.7 V for 5 h are shown in Figures 6−8, respectively. In comparison with Figure 3, the XRD peaks of CdS are more evident at a deposition potential of −0.7 V (Figure 6). Decreasing the deposition potential from −0.65 to −0.7 V caused the contents of both Cd and S to increase, reaching 3.05 and 3.91%, respectively, while their stoichiometric ratio remained approximately equal to 1:1 (Figure 7). Furthermore, from the FE-SEM image (Figure 8a), the CdS deposition layer at the deposition potential of −0.7 V was thickened relative to that in Figure 5. After CdS electrodeposition, the average inner diameter of the tubes was ∼115 nm, suggesting that the CdS coating layer was ∼15 nm thick (the pure TiO_2 NT substrate had an average inner diameter of 145 nm). The tube length remained unchanged after deposition. A cross-section micrograph of the tubes (Figure 8b) revealed that both the inside and outside surfaces of the NT walls were uniformly covered by a deposited sensitization layer (white arrows).

Figures 9−11 show analysis results for the coaxial heterogeneous structure sample obtained at a deposition potential of

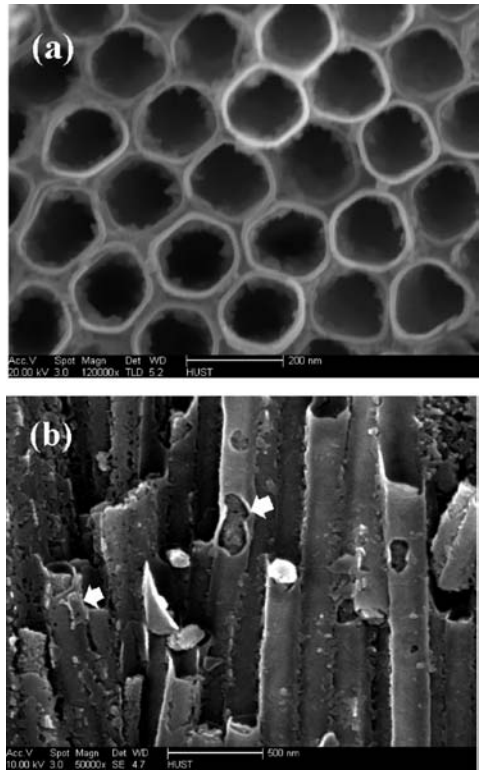

Figure 8. (a) Top-surface FE-SEM micrographs of CdS electrodeposited on TiO_2 NT arrays at −0.70 V (vs Ag/AgCl). (b) Cross-section micrograph of the deposit and substrate.

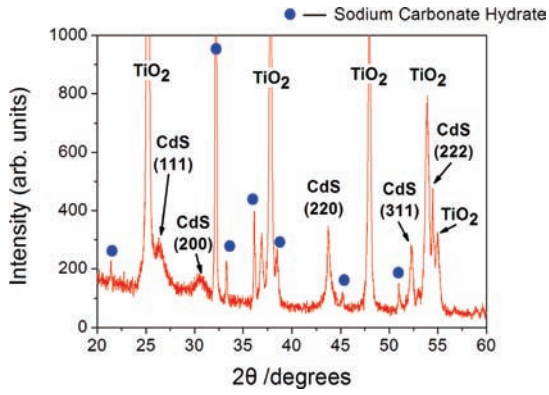

Figure 9. XRD diffractograms of CdS electrodeposited onto TiO_2 NTs at a deposition potential of −0.75 V (vs Ag/AgCl).

−0.75 V after 5 h. Figure 9 shows the XRD pattern of the film sample. At −0.75 V, CdS diffraction peaks continued to strengthen and sodium carbonate hydrate diffraction peaks began to appear. This suggests that the deposition potential of −0.75 V was sufficiently negative that CdS deposition was accompanied by the adsorption of organic complex EDTA. In the subsequent crystallization annealing process (500 °C), EDTA adsorbed onto the sample surface (in the absence of washing with water) decomposed into Na_2CO_3.[68−70] However, the high temperature of 500 °C generally makes it difficult to have hydrated ions. The diffraction peaks of sodium carbonate hydrate that appeared in the XRD pattern may have been due to the strong hygroscopicity of Na_2CO_3. When the annealed samples

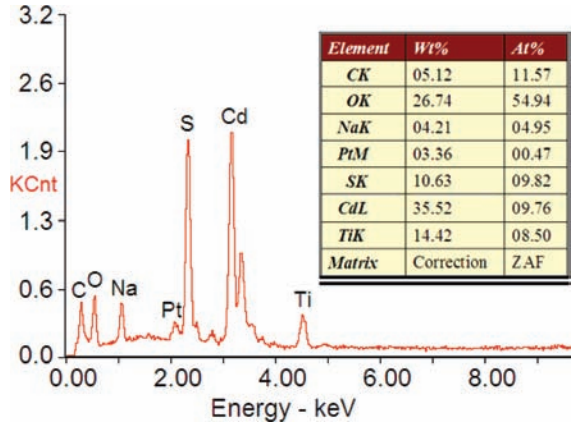

Element	Wt%	At%
CK	05.12	11.57
OK	26.74	54.94
NaK	04.21	04.95
PtM	03.36	00.47
SK	10.63	09.82
CdL	35.52	09.76
TiK	14.42	08.50
Matrix	Correction	ZAF

Figure 10. EDX spectrum of stoichiometric CdS electrodeposited onto TiO_2 NTs at a deposition potential of −0.75 V (vs Ag/AgCl).

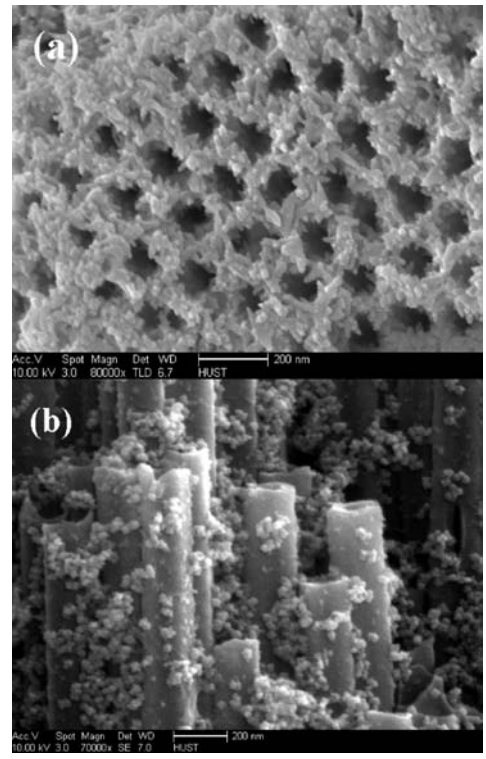

Figure 11. (a) Top-surface FE-SEM micrographs of CdS electrodeposited on TiO_2 NT arrays at −0.75 V (vs Ag/AgCl). (b) Cross-section micrograph of the deposit and substrate.

were transferred for testing, the sodium carbonate on the surface of the samples may have absorbed moisture from the air, forming a sodium carbonate hydrate. Figure 10 shows the EDX spectrum of the film sample. Aside from the continuous increase in the amounts of Cd and S, the spectra of C and Na were also observed at the deposition potential of −0.75 V, indicating the adsorption of organic complex EDTA, which is consistent with XRD results. Figure 11 features FE-SEM micrographs of the film sample, showing the properties of island or particle deposition, which negate the characteristics of the two-dimensional atomic layer deposition of UPD. After CdS electrodeposition, the average inner diameter of the NTs was further reduced, and the distribution became very uneven, making it difficult to accurately measure. Figure 11a shows that some nanoparticles blocked the NT mouths, resulting in a decrease in the specific surface area of the NTs. We found a

(68) Yusufoglu, Y.; Akinc, M. *J. Am. Ceram. Soc.* **2008**, *91*, 77.
(69) Gilbert, E.; Hoffmann-Glewe, S. *Water Res.* **1990**, *24*, 39.
(70) Ku, Y.; Wang, L.-S.; Shen, Y.-S. *J. Hazard. Mater.* **1998**, *60*, 41.

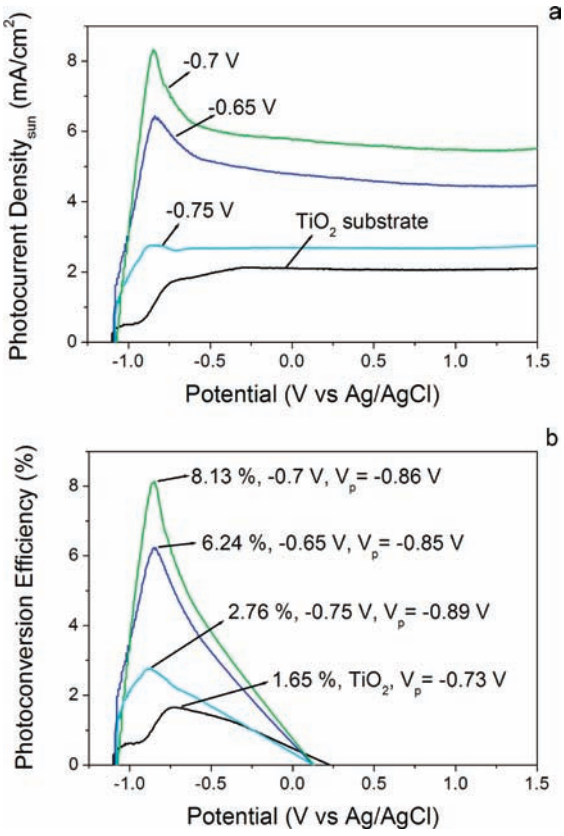

Figure 12. (a) Photocurrent density and (b) corresponding photoconversion efficiency of CdS/TiO_2 nanotube-array coaxial heterogeneous structure samples fabricated using different deposition potentials. The maximum value of the efficiency under 100 mW/cm^2 full-spectrum illumination, 8.13%, was achieved for the sample formed using UPD at −0.7 V.

slight increase in tube length after deposition at −0.75 V, but the increase was very small and within the nanometer scale. Thus, throughout the length of the micrometer range, the tube length can be considered to be almost constant.

Figure 12a shows the measured photocurrent density of samples with the CdS/TiO_2 nanotube-array coaxial heterogeneous structure that were fabricated using the three different deposition potentials; data for the corresponding pure TiO_2 NT substrate before sensitization is also provided. Figure 12b shows the corresponding photoconversion efficiency of the four samples (information regarding the photoelectrochemical measurements and photoconversion efficiency calculations is given in the Supporting Information). The pure unsensitized TiO_2 NT substrate sample achieved a photoconversion efficiency of 1.65%. The photoconversion efficiency increased to 6.24% when the TiO_2 NTs were sensitized by the narrow-band-gap semiconductor CdS at a deposition potential of −0.65 V. At −0.7 V, the photoconversion efficiency reached 8.13%, exhibiting the best visible-light response performance among the samples investigated. A photoactivity value of 8.13% is a 5-fold enhancement compared with that of the pure TiO_2 NTs (1.65%). The value is much higher than the 2.58 and 2.68% levels obtained from CdS-modified TiO_2 NT arrays as reported by Bai et al.[24] and Zhang et al.,[25] respectively. It is second only to Shin et al.'s recent report of 8.5% for CdSe-modified TiO_2 NTs.[29] When the deposition potential was further decreased to −0.75 V, the photoconversion efficiency rapidly dropped to 2.76%, indicating that the coaxial heterogeneous structure had been damaged by the deposition potential. It is highly likely

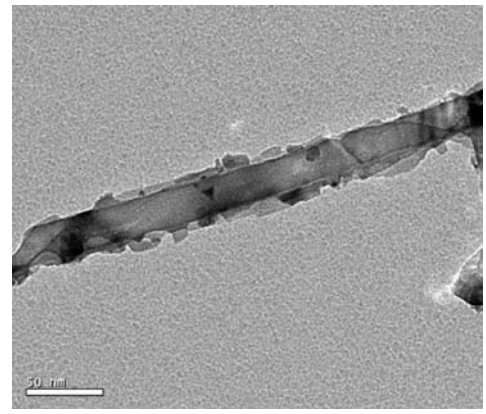

Figure 13. TEM image of a CdS/TiO_2 nanotube-array coaxial heterogeneous structure.

that the nanotube mouth was partially plugged, resulting in a decrease in the specific surface area of the NTs and reducing their photoelectrochemical performance. Incidentally, the value of V_p, the electrode potential (vs Ag/AgCl) of the working electrode at which the maximum photoconversion efficiency was measured, showed a negative shift in the wake of the increase of CdS coverage (negative shift of deposition potential). The precise mechanism of the formation of this trend is currently not well understood. We speculate that the variance in CdS coverage may affect the absorption band of the CdS/TiO_2 coaxial heterogeneous structures, which depends on the contribution of different components of the solar spectrum, thereby causing the V_p to shift. A detailed investigation to determine this is underway.

The prepared CdS/TiO_2 nanotube-array coaxial heterogeneous structures were further investigated using transmission electron microscopy (TEM). Figure 13 shows a TEM image of a single tube wall of the prepared coaxial heterogeneous structure. TiO_2 NTs formed the core material of the wall, which was ∼17 nm thick. From Figure 13, it is evident that the sensitization layer was deposited on both sides of the tube wall of the TiO_2 NT, forming a coaxial heterogeneous structure. It can also be seen that the thickness of the deposited sensitization layer was only ∼10 nm, which is smaller than the value of 15 nm obtained from the FE-SEM measurements. This may be due to the ultrasonic dispersion process in the TEM measurements, in which a number of deposited sensitization layers could be shaken off by ultrasonication.

The photoresponse of the CdS/TiO_2 NTs was determined by potentiostatic [current (I) vs time (t)] measurements under pulsed illumination. Figure 14 shows the $I-t$ curve obtained from a photoelectrochemical cell containing CdS/TiO_2 NTs as the photoanode and Pt as the cathode at a constant potential of 0.5 V (vs Ag/AgCl). The photocurrent value decreased to zero as soon as the incident light on the photoanode was turned off and returned to the original value only when the light was turned on again. This indicates that charge transport in the material proceeds rapidly.

Conclusions

We have reported the conceptual design and a suitable architecture for the composite material formed from self-assembled TiO_2 NTs and the narrow-band-gap compound semiconductor CdS. The novel CdS/TiO_2 nanotube-array coaxial heterogeneous structure films were produced using the electrochemical ALD technique. The modified electrochemical ALD

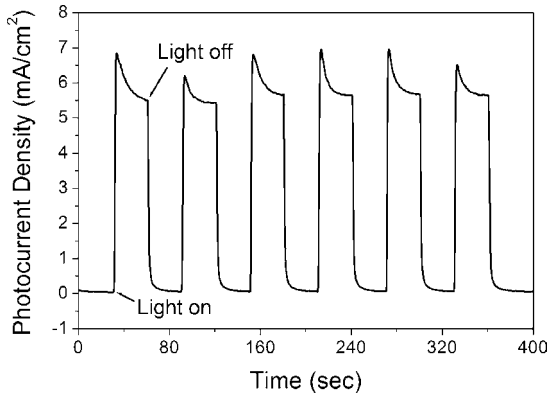

Figure 14. Photocurrent response of a CdS/TiO_2 nanotube-array coaxial heterogeneous structure photoanode to on−off cycles of illumination. The photocurrent became almost zero when the light was switched off (illumination stopped). The original photocurrent returned after illumination.

technique has been shown to be suitable for coating uniform thin films of narrow-band-gap compound semiconductors onto large-surface-area nanostructured substrates. The CdS/TiO_2 composite material architecture demonstrates properties useful for hydrogen generation by water photoelectrolysis. More importantly, we believe that the new electrochemical synthesis technique can be extended to other binary or ternary narrow-band-gap compound semiconductors of interest for water photoelectrolysis and toxic pollutant photocatalytic degradation. Future efforts will focus on optimization studies of the photoactive composite material, including the control of the thickness of the deposited sensitization layer simply by using different deposition times at an optimized UPD deposition potential, as well as the investigation of alternative dopants, such as Pt, Co, V, Ni (metallic doping) or C, N, B (nonmetallic doping) by changing the deposition solution during the electrochemical ALD process.

Acknowledgment. This work was cofinanced by the National Natural Science Foundation of China (20873048, 30970717, 50827204, 50972047), the Research Fund for the Doctoral Program of Higher Education (200804871011), the Program for New Century Excellent Talents in University (NCET-06-0644), and the Cultivation Fund of the Key Scientific and Technical Innovation Project, Ministry of Education of China (707044). Technical assistance from the Analytical and Testing Center of HUST is gratefully acknowledged. The authors also thank the reviewers for their helpful comments.

Supporting Information Available: Experimental section, including the detailed process for preparing the TiO_2 NT substrate. This material is available free of charge via the Internet at http://pubs.acs.org.

JA1025112